nature cancer

Article

https://doi.org/10.1038/s43018-023-00692-y

Multiregion sampling of de novo metastatic prostate cancer reveals complex polyclonality and augments clinical genotyping

In the format provided by the authors and unedited

Supplementary Note

Below is a summary of additional methodology for **Multi-region sampling of *de novo* metastatic prostate cancer reveals complex polyclonality and augments clinical genotyping**

DNA extraction

Cell-free DNA (cfDNA) was extracted from 2-6 mL thawed and vortexed plasma using the QIAGEN QIAamp® Circulating Nucleic Acid Kit (catalog number: 55114). The cfDNA extraction was performed as described in the technical manual (QIAamp® Circulating Nucleic Acid Handbook; version October 2019; section “Protocol: Purification of circulating nucleic acids from 1 mL, 2 mL, or 3 mL serum or plasma”). Component volumes were adjusted for 6mL plasma input. If the plasma input was less than 6 mL, the volume was increased to 6 mL with phosphate-buffered saline. In contrast to the technical manual, samples were incubated for 60 minutes at 60°C in a water bath, and cfDNA was eluted by adding 60 µL nuclease-free water to the QIAampMini Column and centrifuging for three minutes at maximum speed. Following extraction, cfDNA was quantified with the Qubit 2.0 Fluorometer and Qubit dsDNA HS Assay Kit, or the Quantus Fluorometer and QuantiFluor ONE dsDNA system.

Germline DNA (gDNA) was extracted from 100 µL thawed and vortexed white blood cells (WBC) using the Promega Maxwell® RSC Blood DNA Kit (catalog number: AS1400) and the Promega Maxwell® RSC Instrument. Samples were prepared as described in the technical manual (Maxwell® RSC Blood DNA Kit; version 4/18 revision). In contrast to the technical manual, the sample tubes were incubated with closed lids at 56°C for 20 minutes in the Illumina Hybridization Oven. Following extraction, gDNA was quantified with a NanoDrop spectrophotometer.

Formalin-fixed paraffin-embedded (FFPE) DNA was extracted from one to four FFPE tissue punches using the Promega Maxwell® RSC DNA FFPE Kit (catalog number: AS1450) and the Promega Maxwell® RSC Instrument. The FFPE tissue punches were prepared as described in the technical manual (Maxwell® RSC DNA FFPE Kit; version 11/17). In contrast to the technical manual, 400 µL mineral oil was added to the FFPE tissue, and the incubation time at 80°C was increased to five minutes. For a subset of patients without white blood cell aliquots available (n=9), gDNA was extracted from benign prostate tissue selected during pathologist review. Prior to DNA extraction, some FFPE tissue received homogenization with the Precellys Evolution bead mill. However, given a lack of improvement in DNA yield or sequencing data quality (i.e. no differences compared to non-homogenized samples), this was not performed for all samples.

Library preparation

Illumina sequencing libraries for cfDNA samples were made with the KAPA Biosystems KAPA Hyper Prep Kit (catalog number: 7962363001) as described in the technical manual (version

KR0961 – v6.17): 5-500 ng of DNA was input to the library. Custom IDT 10 base pair (bp) Unique Molecular Identifier (UMI) adapters (15 μM) were used for the cfDNA library construction, and the adapters were ligated overnight at 4°C. Beads were resuspended in 25 μL elution buffer (10mM Tris-HCl, pH 8.0-8.5) during post-ligation cleanup, and in 55 μL of nuclease-free water during post-amplification cleanup. The total number of PCR cycles was dependent on the initial DNA input (3-14 cycles).

Illumina sequencing libraries for gDNA samples were made with the KAPA Biosystems KAPA Hyper Plus Kit (catalog number: 07962428001) as described in the technical manual (version KR1145 – v4.17): 50-500 ng of DNA was input to the library. Diluted conditioning solution was used to remove EDTA present at a final concentration of 0.1 mM. Enzymatic shearing of gDNA was performed for 15 minutes at 37°C. Custom IDT 10bp UMI adapters (15 μM) were used for the gDNA library construction, and the adapters were ligated for two hours at room temperature. Beads were resuspended in 25 μL elution buffer (10mM Tris-HCl, pH 8.0-8.5) during post-ligation cleanup, and in 55 μL of nuclease-free water during post-amplification cleanup. The total number of PCR cycles was dependent on the initial DNA input (3-7 cycles). In contrast to the technical manual, the end repair enzyme was heat inactivated at 80°C for 10 minutes prior to the end repair & A-tailing step.

Illumina sequencing libraries for FFPE DNA samples were made with the KAPA Biosystems KAPA Hyper Prep Kit (catalog number: 7962363001) as described in the technical manual (version KR0961 – v6.17): 5-500 ng of DNA was input to the library. FFPE DNA was first mechanically sheared using the Covaris® M220 Focused-ultrasonicator (peak power: 50.0; duty factor: 20.0; cycles/burst: 200; temperature minimum: 18.0°C; setpoint: 20.0°C; temperature max: 22.0°C; required run time: four minutes). Custom IDT 10bp UMI adapters (15 μM) were used for the FFPE DNA library construction, and the adapters were ligated overnight at 4°C. Beads were resuspended in 25 μL elution buffer (10mM Tris-HCl, pH 8.0-8.5) during post-ligation cleanup, and in 55 μL of nuclease-free water during post-amplification cleanup. The total number of PCR cycles was dependent on the initial DNA input (7-17 cycles).

Targeted DNA sequencing

Samples from 43 patients were subjected to targeted sequencing (all FFPE tumor and benign prostate tissue, WBC and cfDNA samples). Targeted sequencing libraries were prepared by using the Roche HyperCap Target Enrichment Kit (catalog number: 08286370001), the Roche HyperCap Bead Kit (catalog number: 08286400001), and a custom Roche SeqCap 73 prostate cancer gene panel as previously published [1]. Targeted enrichment was performed as described in the technical manual (SeqCap EZ HyperCap Workflow User's Guide; version 2.3; chapters five to seven). The amplified captured multiplex DNA sample was resuspended in 53 μL nuclease-free water. In contrast to the technical manual, multiplex DNA sample library pools with a combined mass of 2 μg were prepared. Sequencing was performed on either the Illumina® HiSeq 1500/2500 High Output platform or the Illumina® NextSeq 500 platform. Five samples with less than 50× median sequencing depth were excluded from subsequent genomic and clinical correlative analyses.

Whole-exome sequencing

203 samples across all 43 patients were selected for whole-exome sequencing, such that each patient had one matched primary-metastatic sample pair plus a germline control (where possible). Samples with >20% tumor fraction (from targeted sequencing) were prioritized for exome sequencing. We further prioritized samples deemed most representative of intrapatient heterogeneity based on targeted sequencing genomics (e.g. samples with mutation discordance).

Whole exome libraries were prepared using the Roche HyperCap Target Enrichment Kit (catalog number: 08286370001), the Roche HyperCap Bead Kit (catalog number: 08286400001), and Roche SeqCap EZ MedExome Probes. The targeted enrichment process was performed as described in the technical manual (SeqCap EZ HyperCap Workflow User's Guide; version 2.3; chapters five to seven). The amplified captured multiplex DNA sample was resuspended in 53 µL nuclease-free water. In contrast to the technical manual, multiplex DNA sample library pools with a combined mass of 1 µg were prepared. Sequencing was performed on the Illumina® HiSeq 1500/2500 High Output platform. We excluded four samples due to low sequencing coverage (<20×) and an additional four samples due to pervasive artifacts caused by FFPE oxidative damage.

Combined sample sequencing

Fragmented DNA was treated with NEBNext FFPE DNA Repair v2 (product #: NEB #E7360S/L) to repair FFPE-related DNA damage per section 1 of the manufacturer's protocol. Prior to library preparation (following targeted DNA sequencing protocols described above), DNA extracted from each same-patient tissue region was combined into a single sample. When available, 250 ng of combined DNA was input to each library, otherwise, 100 ng total input was used. Libraries were hybridized to an updated version of our targeted sequencing panel [2].

Targeted DNA sequencing bioinformatics

Mutation calling

Somatic and germline mutations were identified using an established validated pipeline [3]. Briefly, demultiplexed FASTQ files were aligned to the hg38 human reference genome with Bowtie2 [4] with duplicate reads marked using SAMBLASTER [5]. Independent identification of somatic variants required ≥10 supporting reads for both cfDNA and FFPE tumor tissue samples. For DNA extracted from plasma, a minimum variant allele frequency (VAF) of 1% was required. For DNA extracted from FFPE tissue, the minimum VAF threshold was conservatively increased to 8% to mitigate potential false positives due to FFPE-related technical artifacts (i.e. errors resulting from poor-quality DNA). We additionally excluded candidate somatic variants in both cfDNA and tumor tissue that did not meet any of the following criteria: mapping quality ≥15 or ≥30 for coding and non-coding mutations, respectively; read end proximity (i.e. average distance

of the variant from the nearest read end) ≥15 or ≥30 for coding and non-coding mutations, respectively; mutation VAF 10× higher than the matched control sample; mutation VAF >25× or >50× the mutant-specific relative background error rate derived from the pool of all control samples, for coding and non-coding mutations, respectively. Identification of germline variants required ≥8 supporting reads and a VAF >15% in samples serving as the gDNA surrogate (i.e. DNA extracted from leukocytes or histologically benign tissue).

We performed a secondary review of variants that did not meet our minimum VAF or read support thresholds for independent variant calling, but were independently detected in ≥1 other same-patient sample(s) (i.e. tumor-informed variant calling). Dependent variant calls in FFPE used relaxed minimum thresholds of VAF>1% and ≥3 supporting mutant reads and in cfDNA only required ≥3 supporting mutant reads (regardless of VAF).

Copy number evaluation

We used bedtools-2.25.0 to count deduplicated sequencing reads from all targeted or whole-exome capture regions [6]. GC content was calculated for all target regions, and Loess regression was applied to coverage log ratios to correct for GC content bias. Coverage log ratios were calculated against a median reference derived from source-matched tumor-negative samples. We created FFPE and cfDNA-specific median reference profiles from pools of samples with <1% tumor fraction as determined by all orthogonal bioinformatic approaches applied to targeted sequencing data. ctDNA-negative samples were sourced from healthy volunteers. Gene-specific coverage log ratios from targeted sequencing are determined from the median coverage log ratio of all intragenic target regions. We used fixed coverage log ratio thresholds to assign categorical copy number status: (-inf, -1], (-1, -0.3], [0.3, 0.7), and [0.7, inf) represent deep deletion, shallow deletion, copy gain, and copy amplification, respectively. For copy-number calling, combined samples were normalized using a reference profile derived from leukocyte DNA (rather than source-matched FFPE non-tumor material), due to insufficient normal tissue availability for re-sequencing on our updated panel.

Whole-exome sequencing bioinformatics

Mutation calling and copy number evaluation

Whole-exome sequencing (WES) FASTQ files were processed using the identical bioinformatic pipeline as targeted sequencing, including alignment, duplicate marking, and mutation calling. Mutation calling in WES samples used the same pipeline as targeted data and required 8% VAF for FFPE and 2% in cfDNA samples; >8 mutant reads; minimum map quality of 30 and 25 for coding and non-coding mutations, respectively. All other thresholds were identical to methods for targeted sequencing.

Copy number and segmentation were performed as previously described [3]. Briefly, the genome was divided into regularly spaced 1000 bp windows overlapping 50% between consecutive windows. For each window, the number of DNA fragments aligning within the window was

counted using bedtools-2.25.0 [6]. Window counts were then normalized against a reference coverage profile generated from a set of 31 leukocyte DNA and 6 benign FFPE samples, using a custom algorithm accounting for cross-sample GC bias and heterogeneity in global sequencing depth [3]. Windows are excluded if median reference depth is less than 10× or the GC% does not fall within 3-97%. Positional coverage log ratios were calculated by dividing a tumor sample's read count within a window by the corresponding reference coverage, followed by GC correction using the same approach.

To segment the genome into regions with distinct copy number states, we performed a recursive statistical test across each chromosome in each sample. For each chromosome, a breakpoint was identified as the position that maximized the statistical difference between the average coverage log ratios of the aforementioned 1000 bp windows for $L_1,\ldots,L_{a-1}$ and $L_a,\ldots,L_b$, where L is the array of all windows and $1 < a < b < n$. If the statistical difference exceeded a predefined threshold (z-score ≥1.35), a breakpoint was introduced at *a* and the algorithm recursively checked for additional breakpoints in segments $L_1,\ldots,L_{a-1}$ and $L_a,\ldots,L_n$.

Whole-exome sequencing estimation of tumor fraction

For samples that underwent whole-exome sequencing, tumor fraction and ploidy were estimated using genome-wide coverage log ratios and heterozygous single nucleotide polymorphism (SNP) allele frequencies (HSAF) as previously described [3]. Briefly, we tested combinations of tumor fraction and log ratios after performing genome segmentation. For each sample, we initially assumed a diploid model and tested different tumor fraction estimations that maximized concordance between expected and observed exome-wide autosomal coverage log ratios and HSAFs. After determining the diploid model with the best fit, we also generated additional models representing whole genome duplications and triplications. The final model selected minimized error between observed and expected log-ratio and HSAF values. In cases where the optimal model indicated whole-genome duplication, the diploid model generally contained multiple segments with biologically incompatible copy number and HSAF levels (i.e. single copy segments with no HSAF deviation or large segments of zero copies with HSAF deviation).

The expected coverage log-ratio (*LR*) of autosomal chromosomes can be calculated as $LR = log_2[(F * C + (1 – F) * 2) / 2] + D$, where *F*=tumor fraction, *C*=number of copies in cancer cells and *D* is the log-depth ratio representing 2 copies. Calculation of expected HSAF can be expressed as $HSAF = [p*a + (1 - p)*b] / p*c + (1 - p)*D]$, where *p* is tumor fraction, *a* is the number of major alleles, *b* is the major alleles in the normal control (always 1), *c* is the total alleles in the tumor, and *D* is the log-depth ratio representing 2 copies. Derivations of this relationship are used to determine HSAF in instances of copy-loss loss-of-heterozygosity (LOH), copy-neutral LOH, and single-copy gain.

In cases where no tumor was detected using copy number-based approaches, we used a somatic mutation-based tumor fraction estimation as a secondary method. For each sample, we took the set of somatic mutations with ≥30× coverage and in regions where the coverage log-ratio depth was ≤0.3. Assuming the highest VAF mutation represented the 95% quantile

outlier of a binomial distribution (predicated on mutant and total read counts) centered at the true VAF, we then adjusted the VAF down to the median and calculated tumor fraction (*TF*) using the equation *TF = 2/(1+1/(adjusted VAF))*. Estimating ploidy was not possible in the cases where only somatic mutation-based tumor-fraction estimates were available.

Genome-wide copy number comparison between same-patient samples

To evaluate copy number differences between samples, chromosomes were binned into 6 megabase bins overlapping 50% with each adjacent bin. For sections to be included, at least 300 1-kilobase windows must have median reference depth greater than 10× and GC% within 3-97%. Deletions and gains were considered if the rounded estimated copy number was ≤0.5× and ≥1.5× the base ploidy, respectively (to not include single-copy deletion or gains in tetraploid genomes). For alterations to be considered truncal, all evaluable samples within a patient must have a given alteration called at the section. LOESS correction was then used to visualize the trend in copy number changes (**Fig. 3b**, **4e**).

Identification of independent localized tumors

Tumor regions were flagged as putatively independent if they shared few/no somatic mutations (identified from targeted sequencing) detected in another localized tumor region, precluding non-detection due to low tumor fraction. For each flagged case, we then calculated a pairwise mutation concordance ($C = M_s / (M_a + M_b + M_s)$ against every other same-patient primary region for which we had whole-exome sequencing data; M_s are mutations shared between two regions *a* and *b*, whereas M_a and M_b are mutations unique to regions *a* and *b*, respectively. In seven patient tumors, we detected at least one pair of primary tumor regions with a mutation concordance of <0.01, indicating a <1% genomic overlap between these regions. These cases were noted as having putative independent localized tumors.

We required a minimum of 20 evaluable mutations between sample pairs for scores to be included. When determining mutation concordance, M_a and M_b only included mutations that were theoretically detectable in each sample. For each patient mutation, we established the minimum normalized VAF across all samples in which the mutation was detected. Then we calculated the expected VAF in every sample, where for a given sample *a*, the expected VAF can be described as $VAF_{exp} = VAF_{min} \times (TF_a/TF_b)$; TF_b is the tumor fraction of the sample with the lowest observed VAF (VAF_{min}). Using the VAF_{exp} for each sample, we determined the expected mutant read count by multiplying it against the base-specific read depth. For the concordance calculation, we excluded any mutations where the expected mutant read count was <8 (our WES mutation calling threshold) in either of the paired samples.

Sampling multiple biopsies to increase probability of event detection

We performed a sample-without-replacement analysis of all same-patient biopsies to assess increased probability of genotype capture when using >1 sample. The probability of successful event detection (*y*) can be expressed by the following:

$$y = 1 - \left[\frac{C(n,k)}{C((n-x),k)}\right]$$

where *n* is the total number of biopsy samples, *x* is the number of biopsies successfully capturing the event, and *k* is the total number of biopsies analyzed in combination.

Generalizable model of event detection probability via biopsy sequencing

To create a more generalizable model of event detection probability when analyzing multiple samples, we used the following expression:

$$y = 1 - x^n$$

where *y* is the detection probability, *n* is the number of biopsies analyzed, and *x* is a float value between 0 and 1 indicating the fraction of biopsy samples that failed to capture the genotype.

In-silico pooling of primary samples for event genotyping

BAM files of same-patient samples within the selection cohort (see above) were combined using samtools view using only *1/n* random reads from each sample where *n* is the total number of same-patient samples. The combined samples were then run through the same bioinformatic process as above, with the exception of dependent mutation calling. Tumor content was considered the maximum of HSAF- and mutation-based approaches.

References

1. Annala, M. *et al.* Evolution of Castration-Resistant Prostate Cancer in ctDNA during Sequential Androgen Receptor Pathway Inhibition. *Clin. Cancer Res.* **27**, 4610–4623 (2021).
2. Tolmeijer, S. H. *et al.* Early on-treatment changes in circulating tumor DNA fraction and response to enzalutamide or abiraterone in metastatic castration-resistant prostate cancer. *Clin. Cancer Res.* **29**(15), 2835-2844 (2023).
3. Herberts, C. *et al.* Deep whole-genome ctDNA chronology of treatment-resistant prostate cancer. *Nature* **608**, 199-208 (2022).
4. Langmead, B. & Salzberg, S. L. Fast gapped-read alignment with Bowtie 2. *Nat. Methods* **9**, 357–359 (2012).
5. Faust, G. G. & Hall, I. M. SAMBLASTER: fast duplicate marking and structural variant read extraction. *Bioinformatics* **30**, 2503–2505 (2014).
6. Quinlan, A. R. & Hall, I. M. BEDTools: a flexible suite of utilities for comparing genomic features. *Bioinformatics* **26**, 841–842 (2010).

Clinical strata only	Genomic strata only	Integrated clinical and genomic strata
A. High versus low volume (CHAARTED) B. High versus low risk (LATITUDE)	*C. TP53* inactive versus *TP53* intact *D. PTEN* inactive versus *PTEN* intact *E. RB1* inactive versus *RB1* intact	Fig 3g. High risk or *TP53* inactive versus low risk + *TP53* intact F. High risk or *PTEN* inactive versus low risk + *PTEN* intact G. High risk or *RB1* inactive versus low risk + *RB1* intact H. High risk or two of (*PTEN* / *RB1* / *TP53*) inactive versus low-risk + intact in two of three of (*PTEN* / *RB1* / *TP53*)

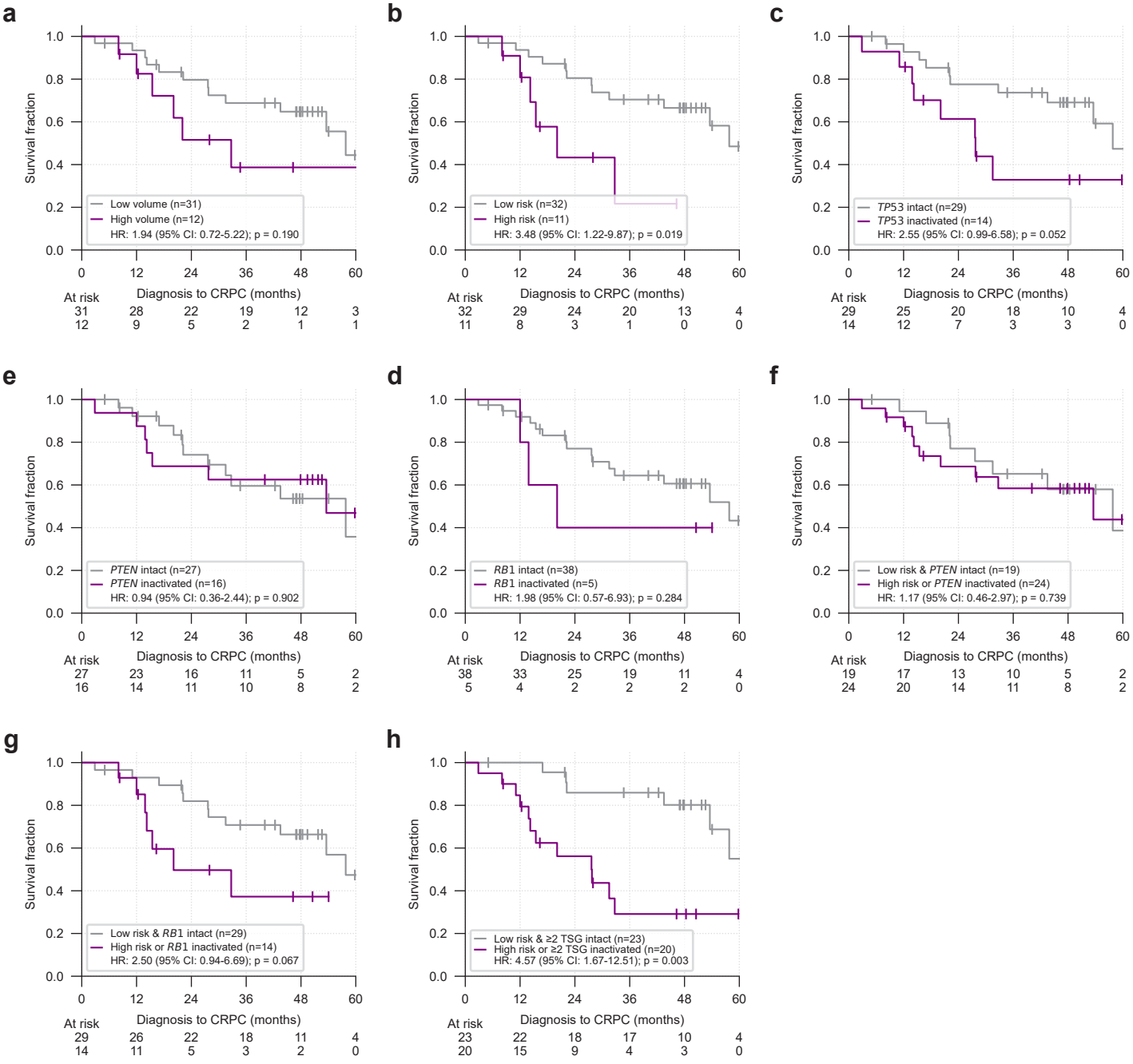

Supplementary Figure 1. Prognostic modeling integrating genomic and clinical characteristics. Kaplan-Meier survival analyses detailing time to castration-resistant prostate cancer (CRPC) from initial prostate cancer diagnosis stratified by clinical and/or genomic characteristics. For all analyses, a patient was considered to have an inactivated gene if a biallelic alteration was identified in at least 1 same-patient sample. To maintain a family-wise error rate <0.05, only unadjusted p-values of less than 0.005 were considered significant (i.e. Bonferroni correction). All p-values produced from Cox Proportional Hazards models are two-sided. TSG: tumor suppressor gene (*PTEN*, *TP53*, and *RB1*).

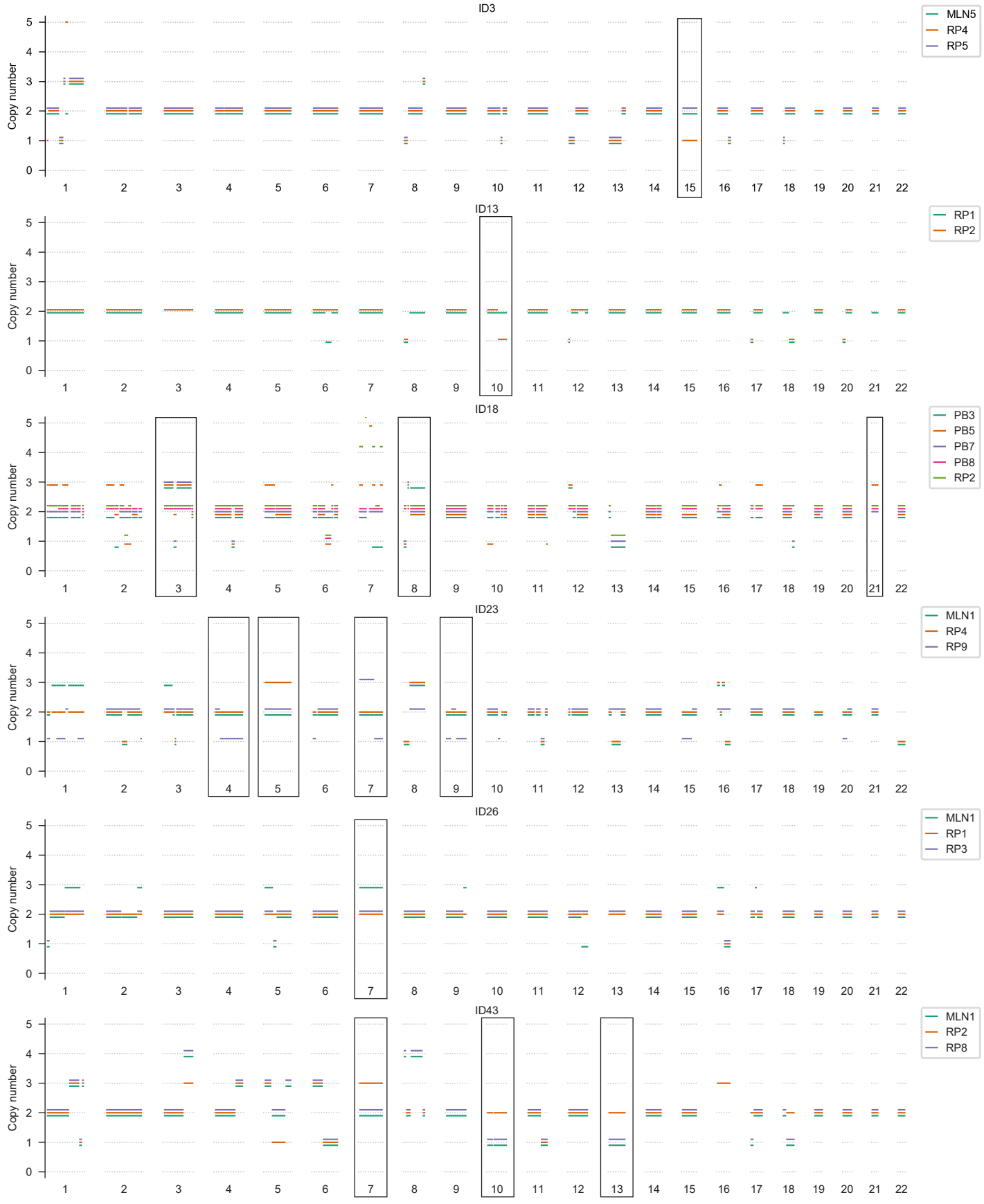

Supplementary Figure 2. Discordant copy number profiles across multiple same-patient tumor samples. Six representative patients with exclusively diploid somatic genomes. Each plot shows chromosomal arm level copy changes for multiple same-patient samples, each denoted by a different color. Heterogeneous large segments in same-patient samples are highlighted in boxes. Only samples with tumor fraction >20% are included. Segment copy number is calculated from coverage log-ratio depth, ploidy, and tumor fraction, and rounded to the nearest integer (**Supplementary Note**). Segments less than 10Mb or with non-integer copy number (remainder between 0.33-0.67) are not shown. ID3, ID13, and ID43 received preoperative androgen deprivation therapy. MLN: metastatic lymph node, PB: prostate biopsy, RP: radical prostatectomy.

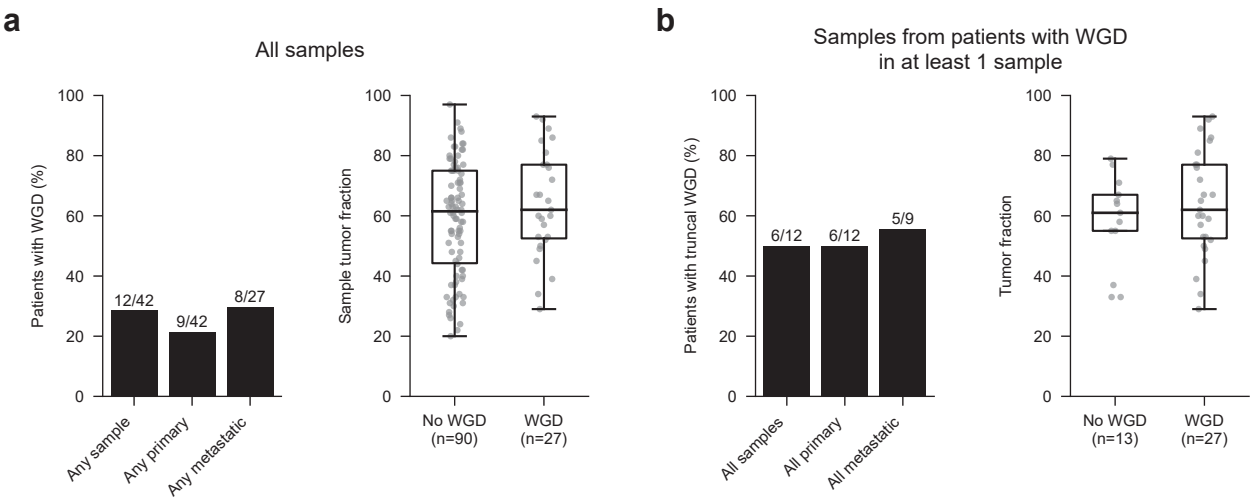

Supplementary Figure 3. Frequency of whole genome duplication and intra-patient heterogeneity. a. Proportion of patients with evidence of whole genome duplication (WGD) in any sample. One patient was excluded due to lack of any sample with sufficient tumor fraction (>20%) for confident WGD inference. Box plot demonstrates that tumor fraction is similar in samples with and without evidence of WGD. Number of independent samples is shown in brackets. b. Patients with WGD detected in at least one sample. In only 50% of patients was the WGD detected in all evaluable tumor samples. Box plot demonstrates that the tumor fraction is similar in diploid and WGD samples from patients with WGD detected in any sample. Number of independent samples is shown in brackets.

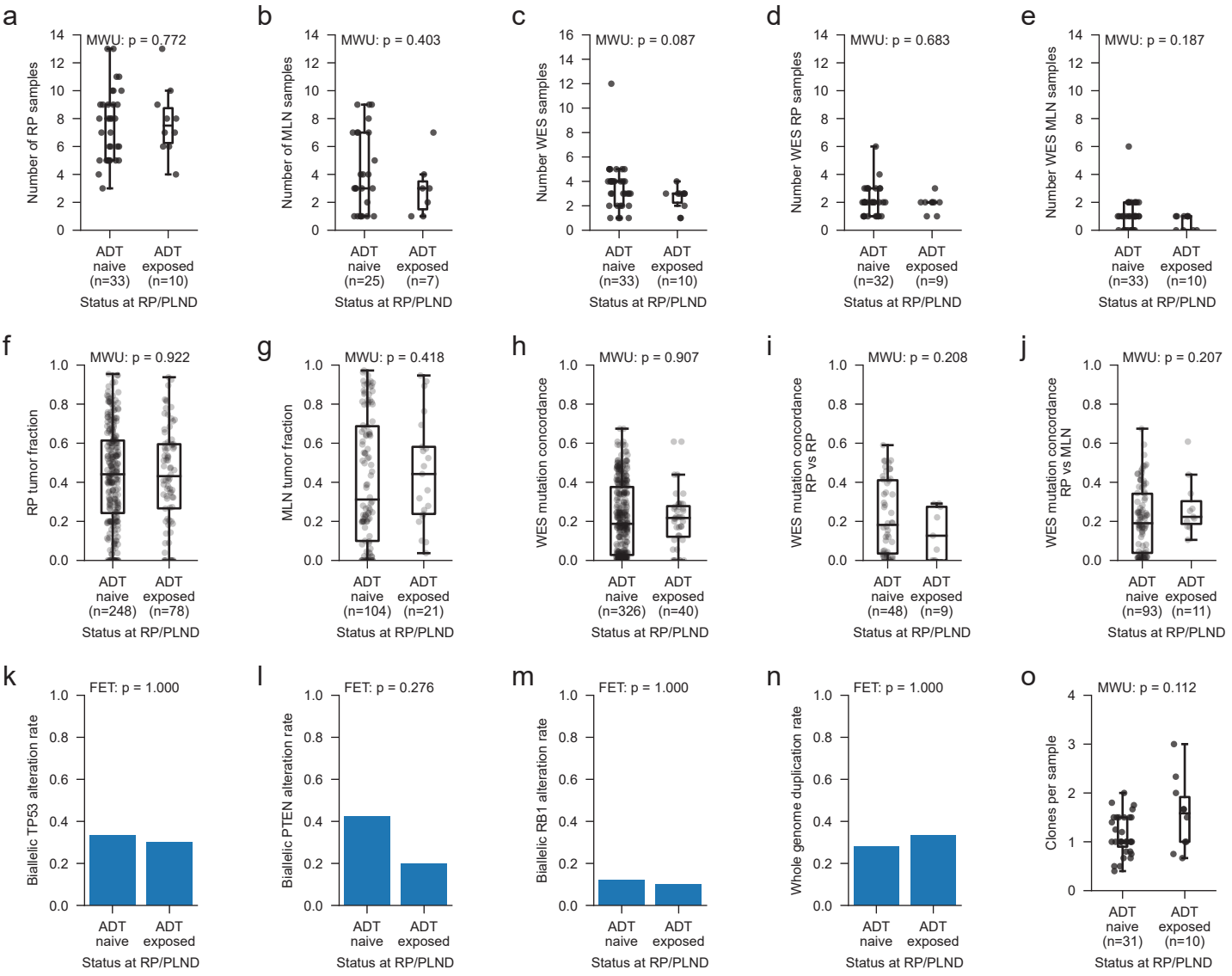

Supplementary Figure 4. Assessment of the effect of androgen-deprivation therapy exposure on clinical and genomic factors. Sample and genomic characteristics of androgen-deprivation therapy (ADT)-naive versus ADT-exposed primary prostate tissue samples. Number of independent patients (**a,b,c,d,e,o**), samples (**f,g**) or same-patient sample pairs (**h,i**) are shown in brackets. FET: Fisher's Exact Test, MLN: metastatic lymph node, MWU: Mann-Whitney U test, PLND: pelvic lymph node dissection, RP: radical prostatectomy, WES: whole-exome sequencing.

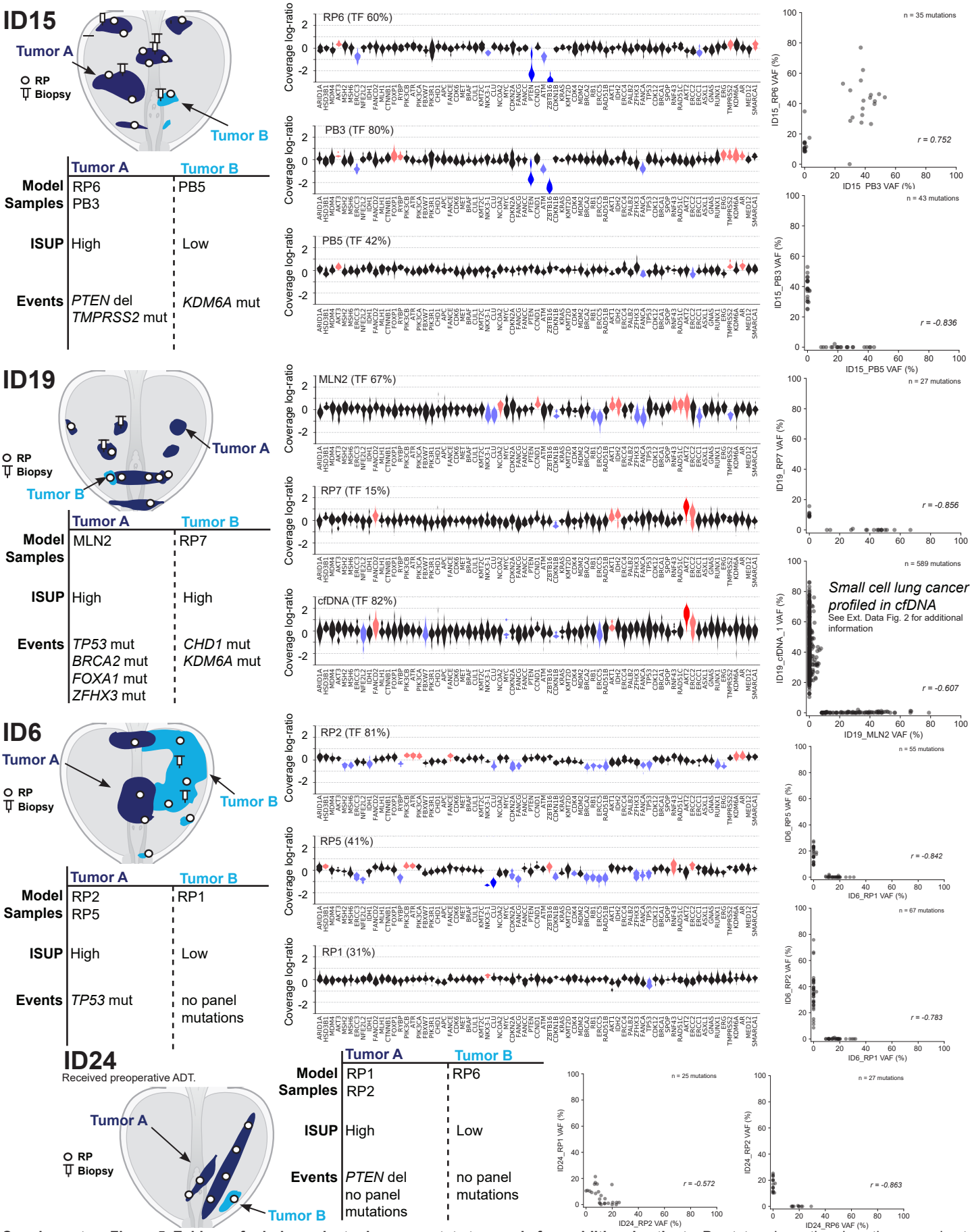

Supplementary Figure 5. Evidence for independent primary prostate tumors in four additional patients. Prostate schematics show the approximate location of profiled prostate biopsy (PB) cores and radical prostatectomy (RP) regions. Estimated extent of tumor involvement (as determined by histopathological review, see **Methods**) is shown, and independent tumors (labeled A, B, and C) are indicated by color. For select representative samples from each independent tumor, the highest observed International Society of Urological Pathology (ISUP) grade and key genomic alterations are shown. Different patterns of copy number alterations in genes (middle) on the targeted panel are shown for selected samples; coloring indicates deep deletion (dark blue), shallow deletion (light blue), copy-neutral (black), copy-gain (red) and amplification (dark red). Scatterplots (right) and Pearson correlation of all mutations detected via whole-exome sequencing in select sample pairs depict no overlap between independent tumors. Del: deletion, Mut: mutation. ADT: androgen-deprivation therapy, TF: tumor fraction, VAF: variant allele fraction.

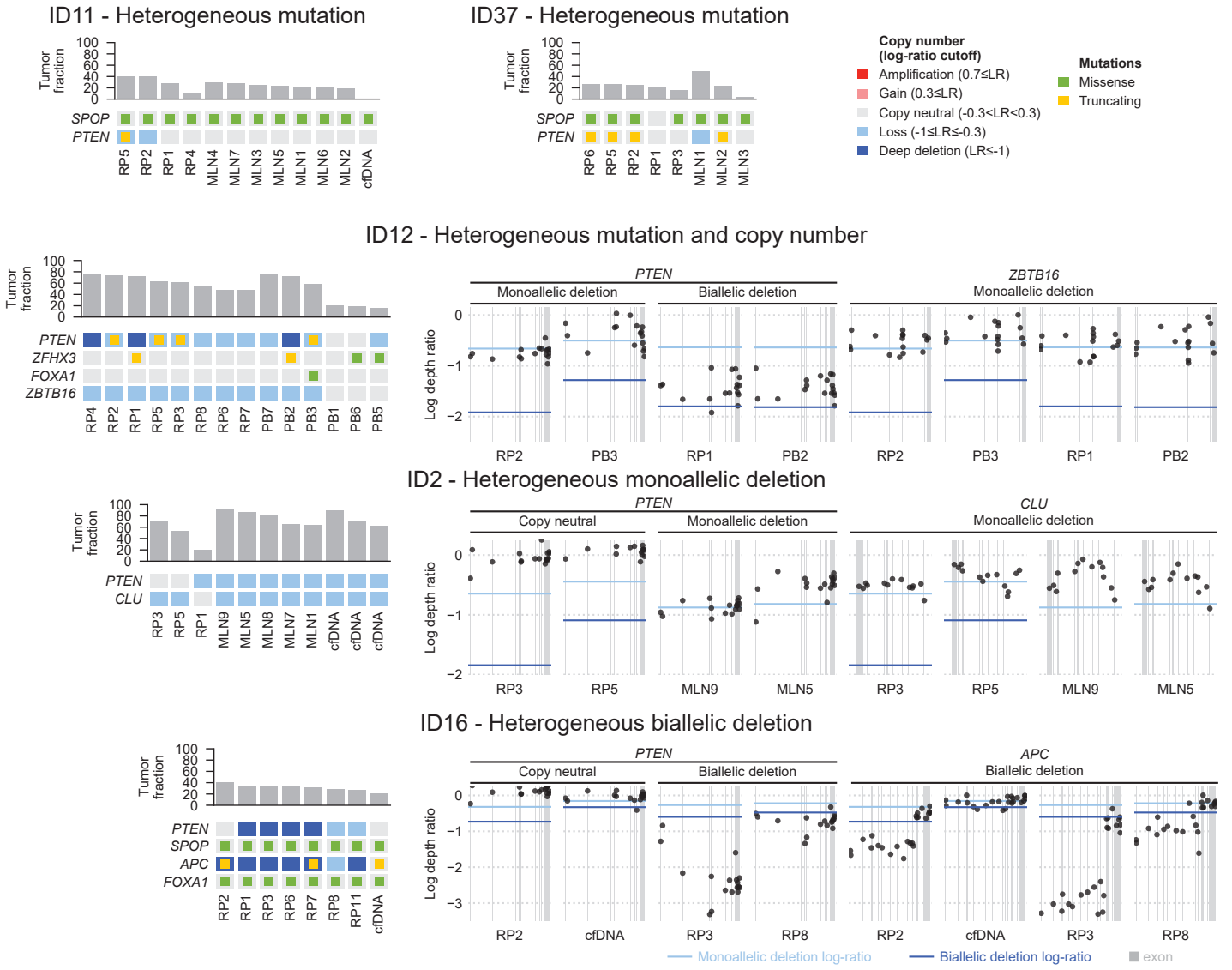

Supplementary Figure 6. Evidence for intratumoral heterogeneity in *PTEN* status. Summary of selected somatic mutations, copy number alterations, and tumor fraction estimates for all samples from five patients with heterogeneous *PTEN* status. In three example cases with heterogeneous *PTEN* copy number status, targeted probe coverage log-ratios (LR) are shown across the *PTEN* gene body with expected coverage log-ratios (given sample-specific tumor fraction) of monoallelic and biallelic deletions shown in light blue and dark blue lines, respectively. An additional gene with truncal copy number alterations is shown (on the right) for comparison, for each patient. Exons are marked in gray vertical lines on the copy number plots. cfDNA: cell-free DNA, MLN: metastatic lymph node, PB: prostate biopsy, RP: radical prostatectomy.

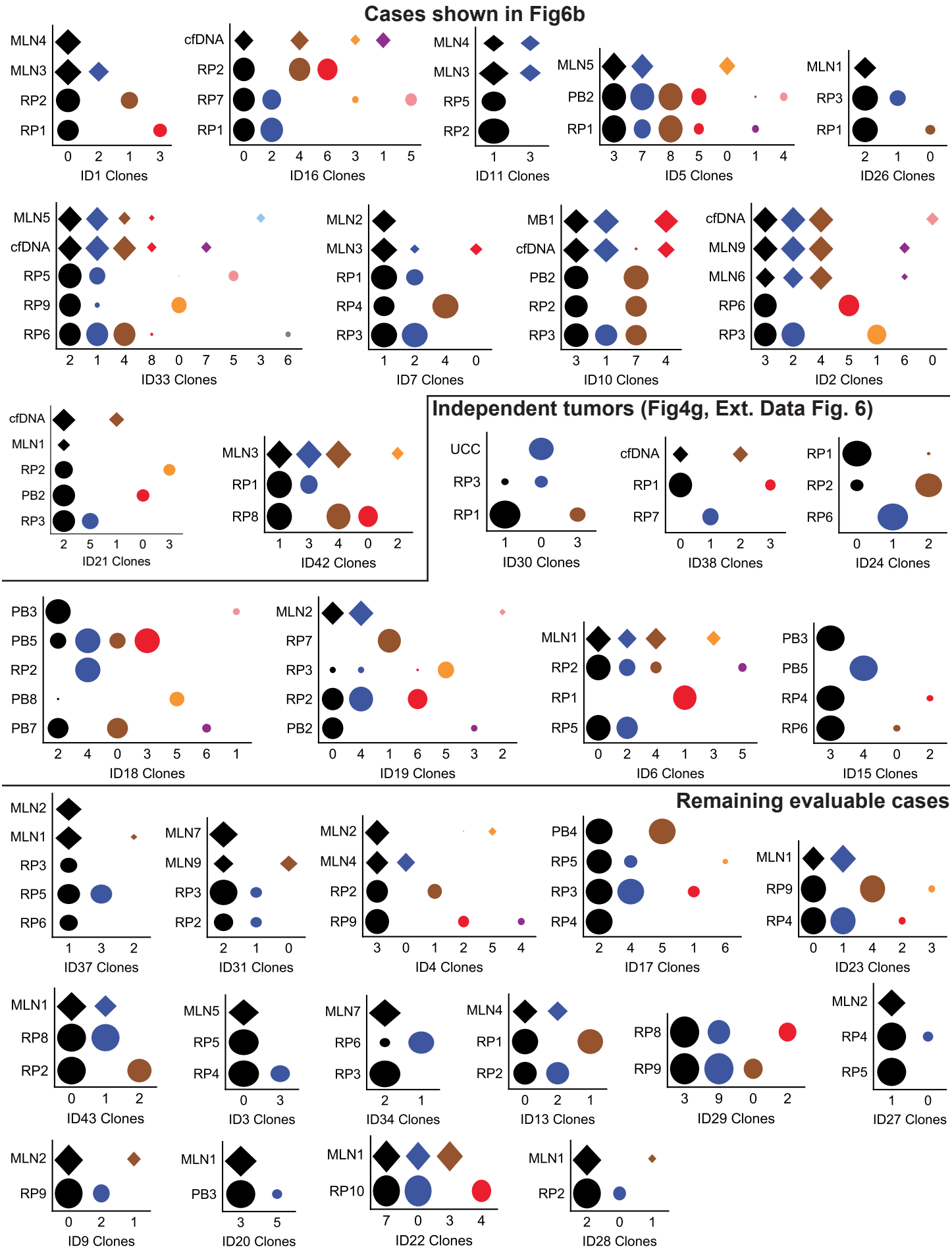

Supplementary Figure 7. PyClone cluster presence and cancer cell fraction in all patients. Matrices showing presence of clones in each sample for each patient. Color indicates PyClone-identified clone assignment, and size represents median cancer cell fraction of mutations within the cluster. Circles and diamonds denote samples from primary and metastatic tumor niches, respectively. X-axis labels denote PyClone-identified clones that passed filtering parameters. Figures are grouped by patients shown in **Figure 6** (top), those with evidence of independent tumors described in **Figure 4g** (middle), and all remaining evaluable cases. Patients with data from only a single sample, a single PyClone-identified clone, and the patient with somatic hypermutation (ID8) are not shown. Sample sources are as follows: cfDNA: cell-free DNA, MLN: metastatic lymph node, PB: diagnostic prostate biopsy, RP: radical prostatectomy, UCC: urothelial carcinoma.

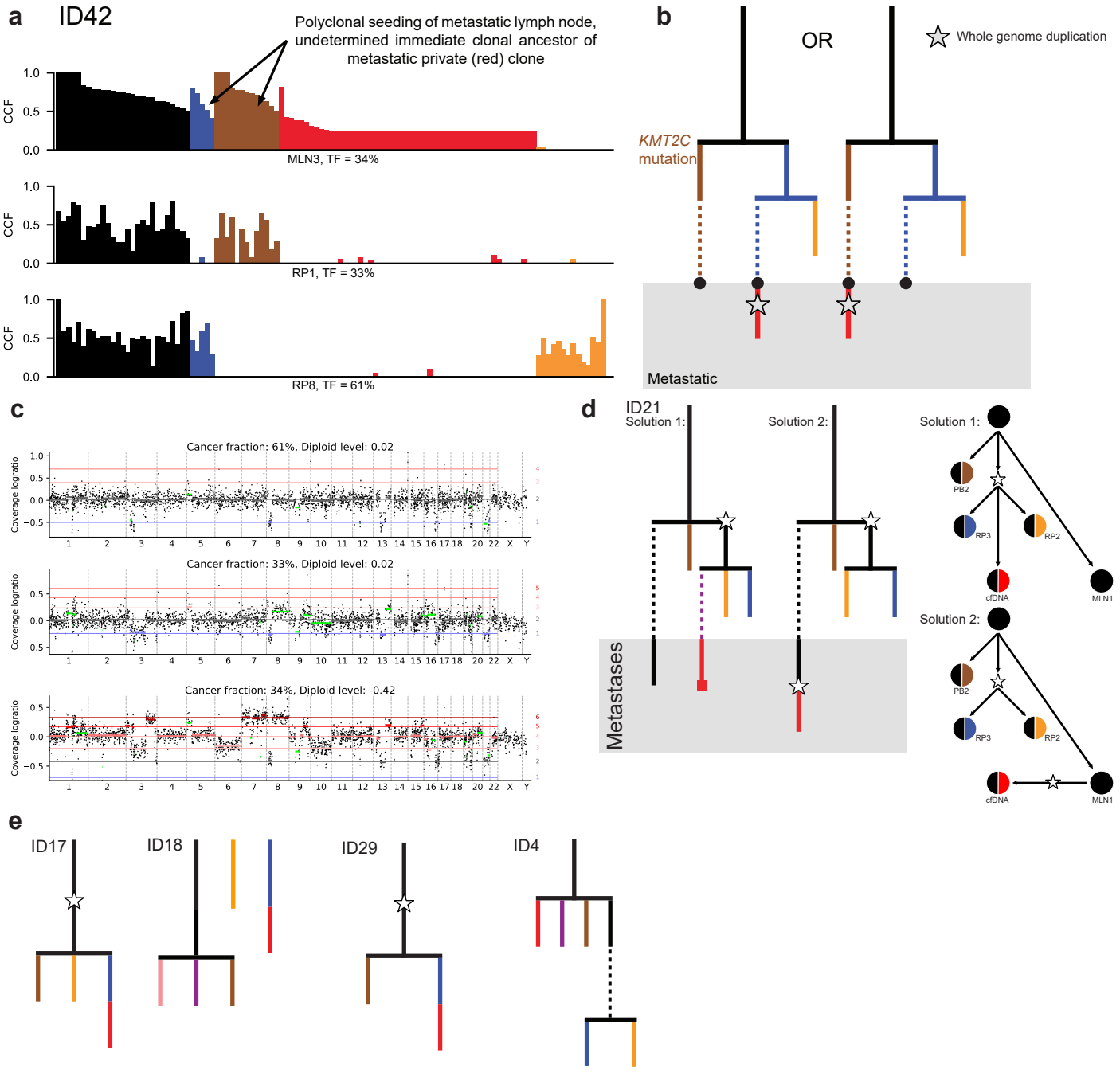

Supplementary Figure 8. Alternative parsimonious phylogenetic solutions in six cases. a. ID42 has a metastatic lymph node with unclear clonal origin. Mutation variant allele fraction (VAF) normalized by tumor fraction (i.e., cancer cell fraction, CCF) and colored by PyClone clone assignment. MLN3 has clonal populations (colored blue and brown) exclusive to RP1 and RP8, respectively. Therefore, MLN3 must have been seeded by separate populations related to those seen in RP1 and RP8. However, the ancestral origins of the red clone are unclear from these data. **b.** Two trees (not shown in Figure 6) are depicted on the right, demonstrating equivalently possible phylogenies. **c.** Coverage log-ratio and segmentation of whole-exome data from ID42. Segmentation coloring reflects absolute copy number. Green segments did not align to our model. **d.** Possible phylogenetic trees and migration graphs for ID21 either with polyclonal dissemination and a single whole-genome duplication (WGD) or monoclonal dissemination and multiple WGD events. **e.** Alternative phylogenetic trees for four additional cases with multiple equivalently parsimonious solutions. cfDNA: cell-free DNA, MLN: metastatic lymph node, PB: prostate biopsy, pre-op: preoperative, **RP: radical prostatectomy, TF: tumor fraction.**

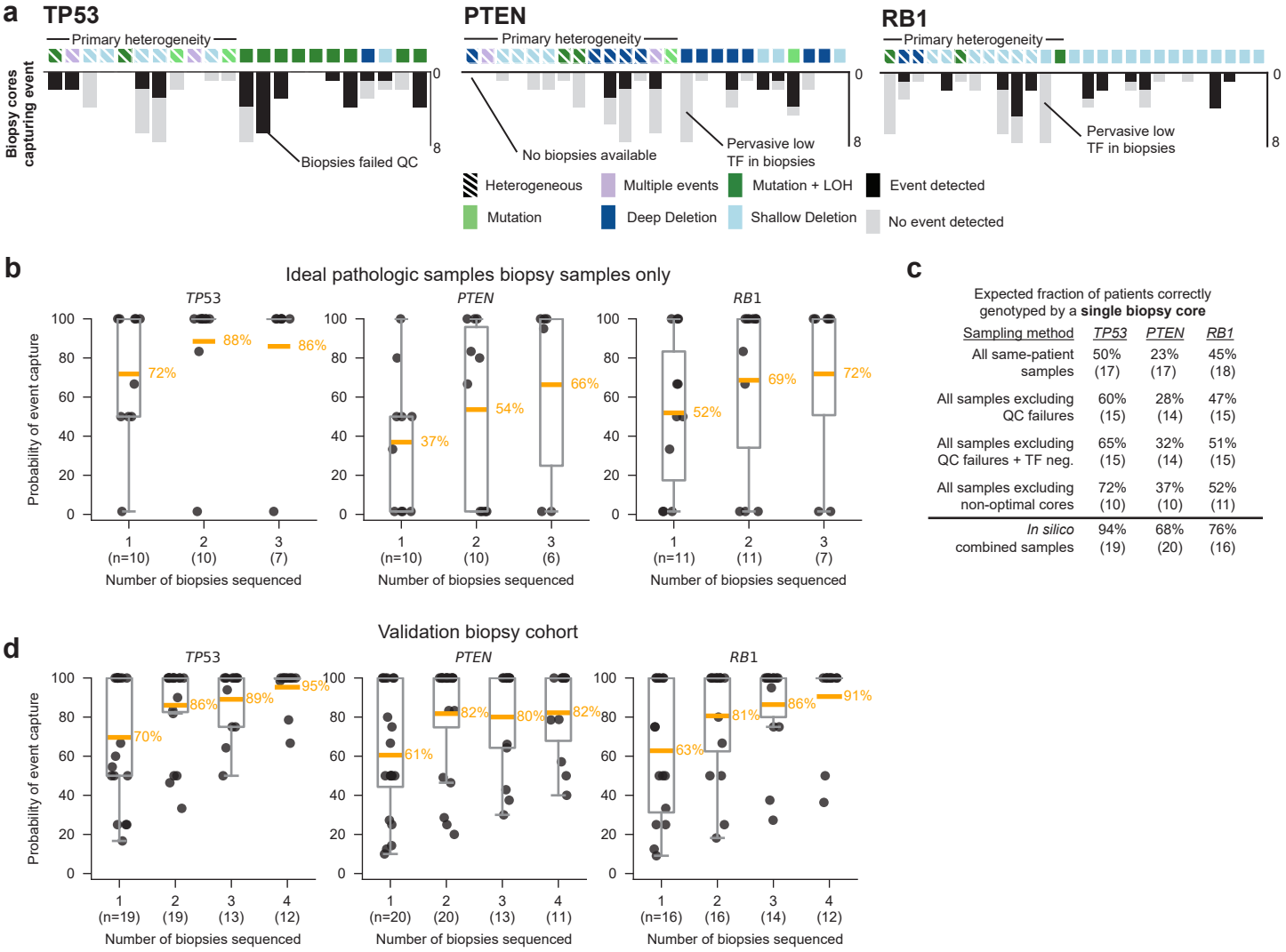

Expected fraction of patients correctly genotyped by a **single biopsy core**

Sampling method	*TP53*	*PTEN*	*RB1*
All same-patient samples	50% (17)	23% (17)	45% (18)
All samples excluding QC failures	60% (15)	28% (14)	47% (15)
All samples excluding QC failures + TF neg.	65% (15)	32% (14)	51% (15)
All samples excluding non-optimal cores	72% (10)	37% (10)	52% (11)
In silico combined samples	94% (19)	68% (20)	76% (16)

Supplementary Figure 9. Limitations of biopsy core sequencing to identify representative tumor suppressor genotypes. a. Fraction of same-patient biopsy cores that successfully captured (black) or failed to capture (gray) representative tumor suppressor genotypes inferred from multiregion profiling of all specimens. The consensus genotype of each patient (column) is shown above, with hatched lines denoting evidence of heterogeneity between same-patient samples. Up to eight biopsy cores were available per patient. **b-c.** Probability of capturing known *TP53, PTEN*, and *RB1* alterations from sequencing same-patient single-biopsy cores as a function of number of cores profiled: (**b**) only utilizing cores with high histopathological tumor cellularity and International Society for Urologic Pathology (ISUP) grade (i.e. analogous to typical clinical workflows omitting poor quality sample material), and (**c**) performed within an independent validation cohort of 129 biopsy cores (excluding samples that failed quality control (QC)) from 34 patients analyzed using the identical bioinformatic methodology as our primary cohort. Final row reflects data from the in silico sample pooling model (**Fig. 7d, Supplementary Note**). **d.** Expected percentage of patients correctly genotyped with a single biopsy core, stratified by sample pool from which a single biopsy core is randomly selected. Parentheticals enumerate the number of patients with known mutations and applicable samples. Increasing detection frequency is due to classifying additional results as failure rather than biomarker negative and does not necessarily increase the number of patients correctly genotyped. Number of evaluable patients in **b** and **d** are shown in brackets. TF: Tumor fraction; LOH: loss-of-heterozygosity.